

Section 9

**Development of and studies with
coupled ocean-atmosphere models**

Global warming and Mean Indian summer monsoon

Sujata K. Mandke^{*1}, A K Sahai¹, Mahesh Shinde¹ and Susmita Joseph¹

¹Climate & Global Modeling Division, Indian Institute of Tropical Meteorology, Pune 411 008, India

*amin@tropmet.res.in

The rising level in concentration of green house gases(GHGs) in the atmosphere have led to enhanced radiative heating of the earth. Global warming is evident from increase in temperature, sea level rise etc(IPCC,1990,IPCC WG1 TAR,2001). The extreme events of climate system such as floods and droughts is projected(IPCC WG1 TAR, 2001). The impact of climate change on monsoon and its variability is a major issue for Indian subcontinent where agriculture and economic growth is strongly linked to behavior of monsoon. Current versions of Atmosphere-Ocean General Circulation Models(AOGCM) provide reliable simulations of the large scale features of the present day climate but there are uncertainties on regional scale. The present study emphasis the possible impact of climate change on the daily mean summer precipitation focusing on Indian region simulated by ten AOGCMs.

Daily precipitation simulated by ten AOGCMs that participated in IPCC for fourth assessment report is used in the present study. The model output from variety of experiments carried out by different modeling groups throughout the world is archived by PCMDI and made available on request to international research community on pcmdi.llnl.gov/ipcc/about_ipcc.php website. Two experiments namely 1pctto2x (1% per year CO₂ increase to doubling) and 1pctto4x (1% per year CO₂ increase to quadrupling) have been used to study the influence of climate change relative to control experiment. The period 1981-2000 from 'climate of the 20th century project(20C3M)' is used as control. In 1pctto2x experiment, CO₂ is increased by 1% per year for 70 years (time of doubling) and with doubled CO₂ additional 150 years run is carried. In 1pctto4x, CO₂ is increased at the rate of 1% per year for 140 years (time of quadrupling) and then an additional 150 years is made with quadrupled CO₂.The details of various model data available for twenty years in 1pctto2x and 1pctto4x experiments that is used in present study is provided in Table-1.

Mean daily precipitation from control simulations are validated with rainfall observations (averaged for 1981-2000) over Indian land prepared by Indian Institute of Tropical Meteorology(IITM) , Pune, India (personal communication, Revadekar) using data of 200 well distributed stations published by India Meteorological Department (IMD) in Indian Daily Weather Report (IDWR). The daily rainfall grid point data on 0.5⁰x0.5⁰ was prepared from station data using inverse distance method. Daily mean precipitation from 16May-15October in 1pctto2x,1pctto4x and 20C3M experiments of ten AOGCMS and IITM observations averaged over central Indian region from 73⁰E-82⁰E; 18⁰N-28⁰N are shown in figure 1(a-j). Observed Mean daily cycle shows normal distribution reaching peak at the end of July. Comparison of control simulations with observation shows that, models underestimate precipitation although the magnitude of underestimation varies from model to model. Among all the models, MIROC3_2_MEDRES best reproduces daily cycle. MRI_CGCM2_3_2a also compares well with observation and only few deficiencies such as late onset and underestimation are found. Few models such as CCCMA_CGCM3_1, ECHAM5/MPI-OM and both versions of GFDL models have double peak during the season. INMCM3.0 and ECHO_G models have peak much latter than observed. The response of mean daily precipitation over central Indian region to increased CO₂ is evaluated by comparing 1pctto2x and 1pctto4x with control simulation. Inter model differences are observed in response to climate change such as couple of models shows more increase in precipitation during later part of the season from mid-August and less increase (ECHO_G and GFDL_CM2.1) or even decrease (ECHAM55/MPI-OM,MIROC3_2_3_MEDRES) till mid-August. Marked increase in mean precipitation throughout the season consistently in both climate change scenarios is observed only in MRI_CGCM2_3_2a model. The increase in 1pctto2x simulation is of slightly lower magnitude than 1pctto4x. In MIROC_2_3_MEDRES, increase is only during peak. GFDL_CM2.0 model does not show any change in both climate change experiments.

References:

IPCC,1992: The supplementary Report to the IPCC,1990,Scientific assessment, WMO-UNEP, Cambridge University press, Cambridge,200pp.

IPCC, 2001: Climate change 2001;The scientific basis. Contributions of working group I to third assessment report of IPCC(J.T. Houghton et al) Cambridge University press, Cambridge, UK and New York,NY,USA,881 pp

Table 1 : Details of model integration period considered for analysis

Sr. No.	Model	1pctto2x		1pctto4x	
		First 20-years	Last 20-years	First 20-years	Last 20-years
1	GFDL_CM2.0	---	2061-2080	---	2131-2150
2	GFDL_CM2.1	---	2061-2080	---	2131-2150
3	MRI_CGCM2_3_2A	2001-2020	---	2071-2090	---
4	MIROC3_2_MEDRES	---	2051-2070	---	2121-2140
5	CCCMA_CGCM3_1	---	2050-2069	---	2120-2139
6	ECHAM5/MPI-OM	---	2061-2080	---	2131-2150
7	GISS_e_r	2101-2120	---	2171-2190	---
8	IPSL_CM4	---	2061-2080	---	---
9	INMCM3.0	---	2071-2090	---	2141-2160
10	ECHO_G	2051-2070	2261-2280	2121-2140	2261-2280

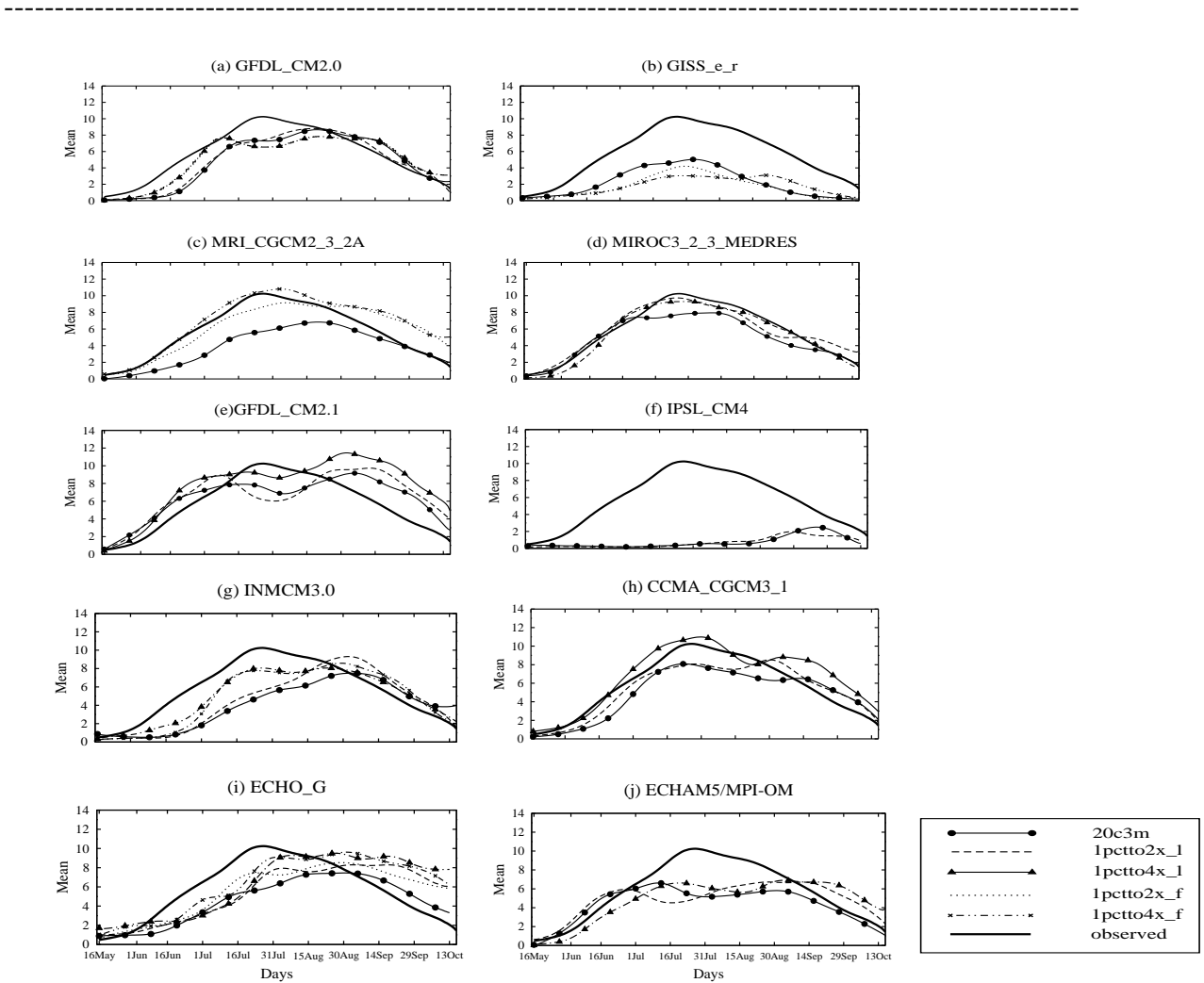


Figure 1: Daily precipitation climatology

Northern Hemisphere extra-tropical cyclone activity in 1961-1990: Comparison of the CGCM3 with the NCEP/NCAR reanalyses

Milka Radojevic, Peter Zwack and René Laprise
Department of Atmospheric Sciences, UQÀM, Montréal, Québec, Canada.

Extra-tropical cyclonic circulation systems induce substantial transport of water vapour, heat and momentum, thus contributing to the maintenance of the time-averaged general circulation of the atmosphere. General circulation models (GCMs) are useful tools for studying a wide range of interacting physical processes that characterize the climate system. Comparison of model simulations with observations provides insights that can aid interpretation of climate variability and future climate-change projections.

The goal of this study is to assess the degree to which the third generation of the Canadian Coupled (atmosphere-ocean) General Circulation Model (CGCM3) replicates extra-tropical cyclone behaviour in the recent climate. An analysis approach was used to identify and track extra-tropical cyclones, and then to compare their statistics over a 30-year period. The statistical method used here includes the computation and mapping of climatological seasonal or monthly means and their standard deviations for various measures of cyclonic activity.

The use of cyclone system climatology for validation is based on the automated objective synoptic systems identification and tracking algorithm of Sinclair (1994, 1997), who was adapted at UQÀM by Rosu (2005). Cyclones are here identified as local maxima of gradient-wind vorticity (ζ_{gr}) computed as the Laplacian of the gridded 1000-hPa geopotential. The use of vorticity captures preliminary stages of large-scale cyclones that would not be detected as pressure minima. Only centres poleward of 20° latitude are included because the gradient wind approximation is not valid close to the equator.

The tracking procedure follows the scheme of Murray and Simmonds (1991a). Tracking attempts to match cyclones at a time with centres at the next analysis time, 6 h later. The chosen combination of matches is one that minimizes a weighted sum of absolute departures of location, pressure, and vorticity from extrapolated values. In order to locate cyclone centres accurately between grid points, a bicubic spline interpolation has been employed. A Cressman filter (see Sinclair, 1997) was applied several times through the algorithm.

The CGCM3 uses the same ocean component as the earlier version, but a new updated atmospheric component, AGCM3. It is a spectral model with triangular truncation at wave number 47 and 32 levels in the vertical on hybrid coordinates. For this study,

model data were first interpolated to pressure levels on a 2.5° lat × 2.5° long grid. The 1000-hPa geopotential was calculated from the model's orography, surface pressure and temperature fields.

The observation-based data used for the comparison/validation are the National Centers for Environmental Prediction and National Center for Atmospheric Research (NCEP/NCAR) reanalyses. The 1000-hPa geopotential from the NCEP/NCAR reanalyses was available on a 2.5° × 2.5° latitude-longitude grid. Model and reanalysis data covering the period 1960 to 1990, four times per day, were then interpolated on a northern hemispheric polar-stereographic grid (97 × 97 points) with a spacing of 180 km at 60° lat.

The algorithm provides information about each cyclone track for a selected period (month, season): date/time, number of centres, their location, and the corresponding ζ_{gr} , cyclonic circulation, and associated precipitable water vapour who is introduced in the algorithm during this study.

In order to eliminate weak perturbations and quasi stationary centres from the cyclone statistics, we imposed following conditions: 1) threshold of ζ_{gr} is $2.5 \cdot 10^{-5} \text{ s}^{-1}$, 2) minimum track lifetime is one day, 3) total track length is at least of 1200 km, and 4) minimal distance between final and initial track positions is at least of 600 km.

The measure of cyclone distribution presented here is track density, defined as the number of discrete cyclone tracks passing within 333 km of any grid point. It is obtained by counting the centres just once per track per grid point. This requires cyclones positions to be related into tracks. Because of the overlapping area(s) between neighbouring search circles, one cyclone track may be taken into account at several grid points at the same time.

Fig. 1 shows the NH geographical distribution of the climatological mean of cyclone track density from November to April (NDJFMA). The NCEP/NCAR reanalyses (Fig. 1a) reveal two regions of pronounced maxima. The first extends from Japan toward the Gulf of Alaska, while the second extends from the Great Lakes and North American East Coast, across the North Atlantic and into Sub-Arctic Ocean. Secondary maxima occur over the northern Eurasia and the Gulf of Genoa. Comparison with the results from the CGCM3 (Fig. 1b) confirms this general picture of cyclonic activity, but with a slight under-estimation in

the polar region and a larger over-estimation in the oceanic regions of maxima (see Fig. 1c).

Fig. 2 shows the NH geographical distribution of the standard deviation of seasonal-mean cyclone track density for the same period. Results from CGCM3 (Fig. 2b) show a great similarity to those of NCEP/NCAR reanalyses (Fig. 2a). The greatest interannual variability of the track density around the seasonal-mean climatological average occurs in the preferred cyclone regions such as Iceland, the Gulf of Genoa and the East China Sea. The main differences between two distributions of variability (Fig. 2c) occur in the same regions as those seen in the means.

Therefore, in comparison with the NCEP/NCAR reanalyses, the CGCM3 simulations reproduce well the statistics of extra-tropical mobile cyclones, with slightly larger averages of winter season track density (Table 1) and their variability.

NCEP/NCAR	CGCM3
24 183	24 260

Table 1. Total number of cyclone tracks over the 30 extended winter seasons (NDJFMA, 1960/61 to 1989/90).

References

- Murray, R. J., and I. Simmonds, 1991:** A numerical scheme for tracking cyclone centers from digital data. Part I: development and operation of the scheme. *Aust. Met. Mag.*, **39**, 155 – 166.
- Rosu, C., 2005 :** Les caractéristiques des cyclones et l'apport d'eau dans les bassins versants du Québec, Master Thesis, Department of Atmospheric Sciences Montréal, UQAM, 132 pp.
- Sinclair, R. M., 1994:** An objective climatology for the Southern Hemisphere. *Monthly Weather Review*, **122**, 2239 – 2256.
- Sinclair, R. M., 1997:** Objective identification of cyclones and their circulation, intensity, and climatology. *Weather and Forecasting*, **12**, 595 – 612.

(www.cccma.bc.ec.gc.ca/models/cgcm3.shtm)

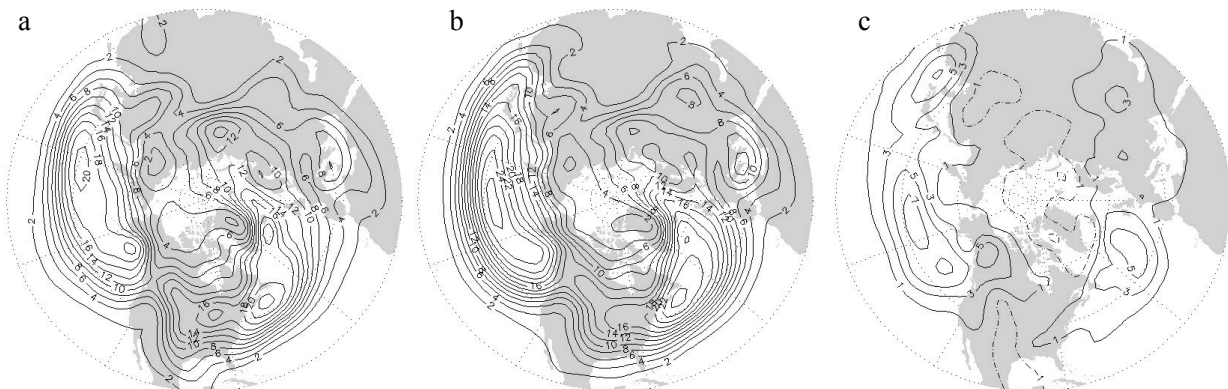


Fig. 1. Mean of extended winter season (NDJFMA) cyclone track density for the NH. Contour interval every 2 centres per 333 km circle per season. (a) NCEP/NCAR, (b) CGCM3 and (c) Difference CGCM3 minus NCEP/NCAR (solid lines for positive differences and dashed lines for negative differences).

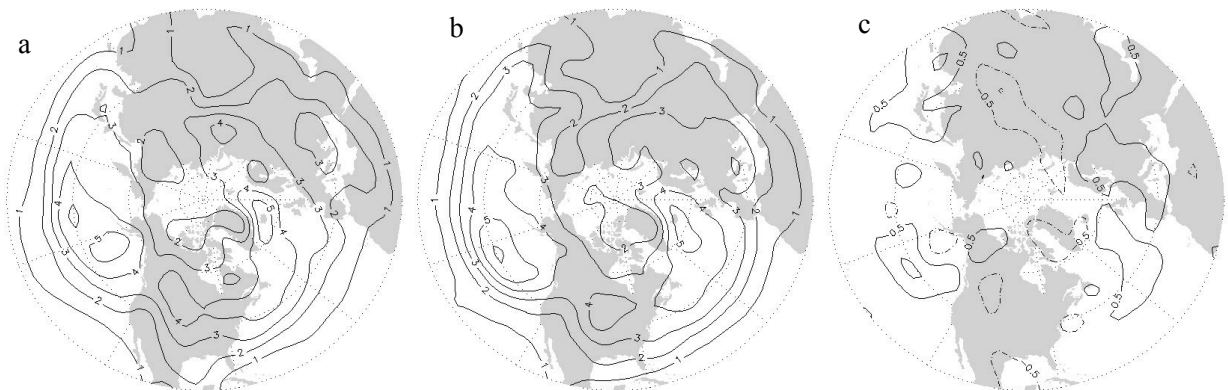


Fig. 2. As above, but for the standard deviation of seasonal mean cyclone track density. Contour interval every 1 centre per 333 km circle per season for (a), (b) and (c).

Impact of enhanced greenhouse gases on Northern Hemisphere extra-tropical cyclone activity in 2041-2070 as simulated by the CGCM3

Milka Radojevic, Peter Zwack and René Laprise

Department of Atmospheric Sciences, UQÀM, Montréal, Québec, Canada.

General circulation model (GCM) projections indicate that enhanced greenhouse gases (GHG) will result in a warming of the lower troposphere particularly, in the polar regions, in winter, over the continents. The reduction of the pole to equator low-level temperature gradient is expected to influence the distribution of extra-tropical cyclones. The goal of this study is to investigate the possible effect of increasing GHG on the climatology of NH extra-tropical migratory cyclones using the simulations of the third-generation Canadian Coupled (atmosphere-ocean) General Circulation Model (CGCM3).

An analysis approach is used here to identify and track extra-tropical cyclones, and then to compare their seasonal statistics over a 30-year model simulation. The cyclone climatology is based on the automated objective synoptic systems identification and tracking algorithm, developed by Sinclair (1997). Cyclones are here identified as local maxima of gradient-wind vorticity (ζ_{gr}) computed as the Laplacian of the gridded 1000-hPa geopotential (for more details, see the companion contribution on the CGCM3 validation in this book).

The atmospheric component of CGCM3 is a spectral model with triangular truncation at wave number 47, and with 32 levels in the vertical on hybrid coordinates. The model projection under investigation corresponds to the period 2040 to 2070, with the Intergovernmental Panel on Climate Change Special Report on Emissions Scenarios (IPCC SRES) A2 scenario forcing. The control simulation covers the period 1960 to 1990.

In order to eliminate weak perturbations and quasi-stationary centres from the cyclone statistics, we imposed following conditions: 1) threshold of ζ_{gr} is $2.5 \cdot 10^{-5} \text{ s}^{-1}$, 2) minimum track lifetime is one day, 3) total track length is at least of 1200 km, and 4) minimal distance between final and initial track positions is at least of 600 km. The cyclone centre density is defined as the number of discrete cyclone centres passing within 333 km of any grid point. Because of the overlapping area(s) between neighbouring search circles, one cyclone centre may be taken into account at several grid points at the same time. A cyclone is considered as intense if its central ζ_{gr} is at least $6 \cdot 10^{-5} \text{ s}^{-1}$. The location of cyclone genesis and lysis corresponds to the initial and final track positions, respectively.

According to the results shown in the Table 1, the total number of both, cyclone occurrences and

cyclone tracks, over the 2040-70 period, is slightly reduced, by about 2%, compared to the control run. Thus, it seems that the enhanced- CO_2 climate is less favourable for the extra-tropical cyclones formation.

Since the geographical distribution of the frequency of cyclone genesis density remains mainly unchanged under the warmer climate, only the results from the control run and the differences are presented (Fig. 1). In winter (DJF), genesis maxima are located along southern part of the North Pacific, east of the Rocky Mountains, the North American East Coast and the Tyrrhenian Sea (Fig. 1a). During the summer (JJA), the genesis maxima are shifted north-eastward (Fig. 1c). In the warmer climate, the cyclone density becomes less frequent everywhere on the NH, in the winter (Fig. 1b) as in the summer (Fig. 1d).

The NH winter frequency of cyclone density in the enhanced- CO_2 climate (Fig. 2a.1), is shifted northward in the north-eastern Canada (the Nunavut Territory) and in the Mediterranean Sea, and is reduced in the Gulf of Genoa, compared to the control climate (Fig. 2b.1). The greatest winter frequency of density of intense cyclones, extending from the Japan to the Gulf of Alaska, shows a minor eastward shift (Fig. 2d.1) in comparison with the control climate (Fig. 2e.1). During the NH summer, there is no change in the cyclone density as in the density of intense cyclones (Fig. 2d.2 and Fig. 2e.2). There are no significant changes in the other averaged cyclone characteristics such as lifetime, speed, central ζ_{gr} , cyclone circulation and precipitable water vapour.

In the enhanced- CO_2 climate, generally, the activity of the NH extra-tropical mobile cyclones slightly decreases in the mid-latitudes, while it increase in the high latitudes near the continents (Fig. 2c.1, 2f.1, 2c.2 and 2f.2). The results here confirm overall those of Lambert and Fyfe (2006).

Reference

Sinclair, R. M., 1997: Objective Identification of Cyclones and Their Circulation Intensity, and Climatology. *Weather and Forecasting*, 12, 595 – 612

Lambert, S.J., and J.C. Fyfe, 2006: Changes in Winter Cyclone Frequencies and Strengths Simulated in Enhanced Greenhouse Warming Experiments: Results from the Models Participating in the IPCC Diagnostic Exercise. *Climate Dynamic* (in press).

(www.cccma.bc.ec.gc.ca/models/cgcm3.html)

(www.cccma.bc.ec.gc.ca/data/cgcm/cgcm_forcing.shtml)

	Control run: 1960 - 1990	Enhanced-CO ₂ run: 2040 - 2070
Winter (December-February)	146 672 (11 919)	143 932 (11 627)
Summer (June-August)	137 982 (12 418)	134 282 (12 184)

Table 1. Total number of NH extra-tropical cyclone occurrences (**tracks**), poleward of 20°N, over the 30 winters and summers.

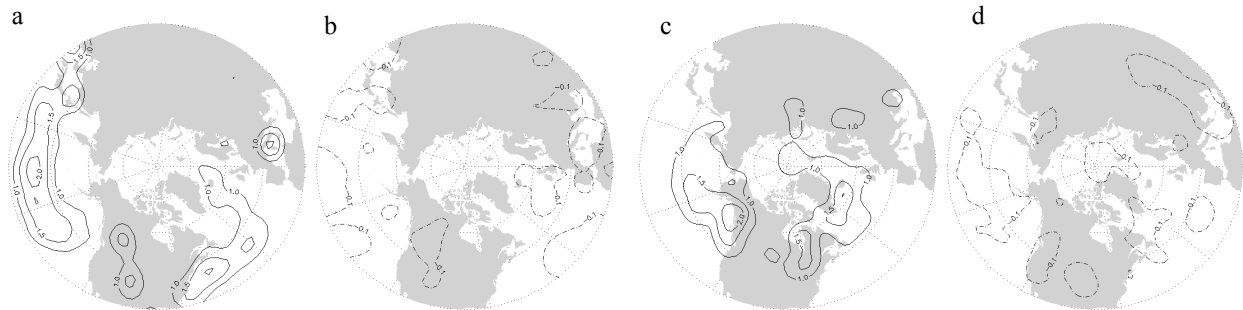


Fig. 1. Mean of extended NH winter (DJF) cyclogenesis density for (a) control, (b) enhanced-CO₂ minus control; (c)-(d) as for (a) and (b) except for the summer (JJA). Contour interval every 0.5 centre per 333 km circle per season for (a)-(d). Solid lines for positive differences and dashed lines for negative differences.

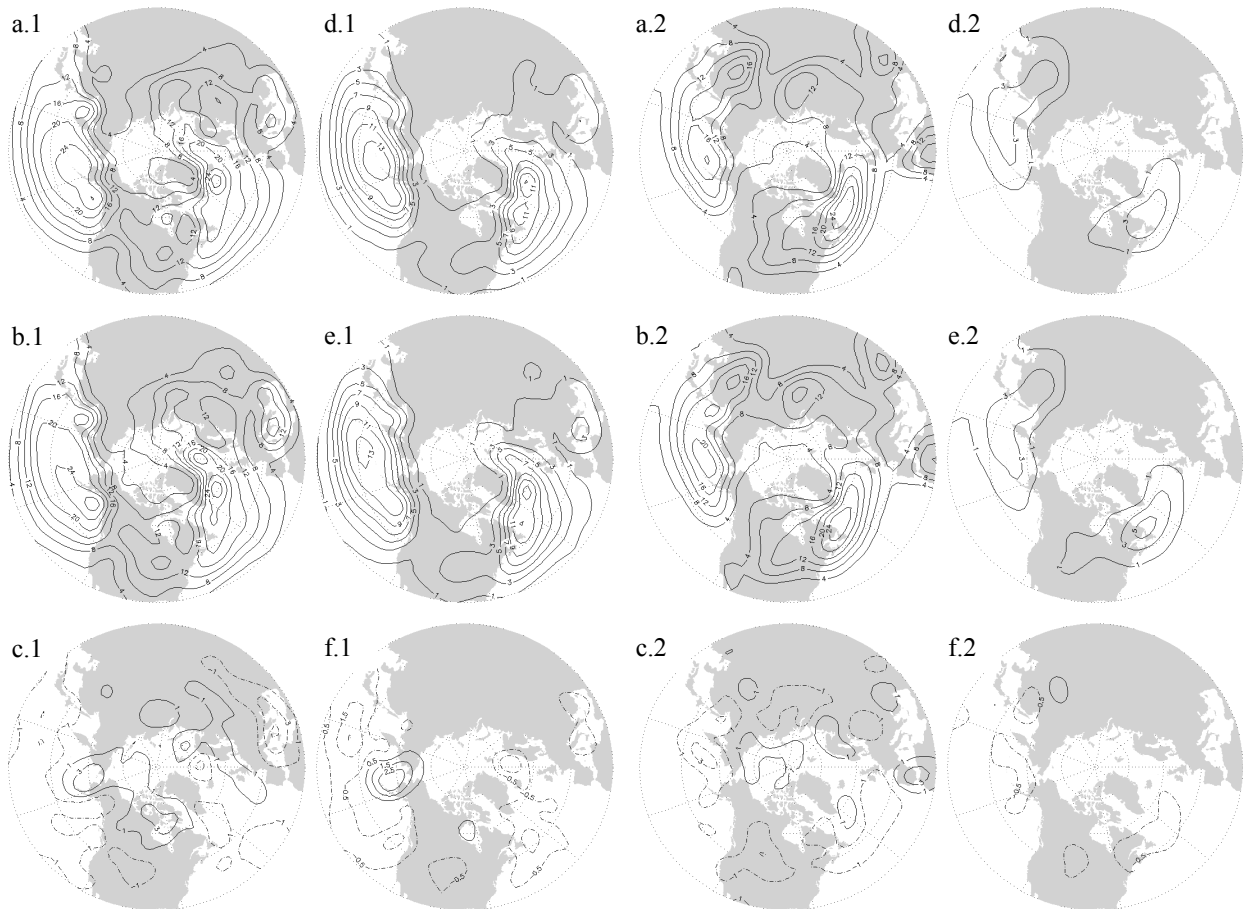


Fig. 2. Mean of NH winter (DJF) cyclone density for (a.1) enhanced-CO₂, (b.1) control and (c.1) enhanced-CO₂ minus control, respectively; (a.2)-(c.2) as for (a.1)-(c.1) except for summer (JJA). (d.1)-(f.1) as for (a.1)-(c.1) except for the intense cyclones; (d.2)-(f.2) as for (d.1)-(f.1) except for the summer (JJA). Contour interval every 4 centres for (a.1), (b.1), (a.2) and (b.2), every 2 centres for (c.1), (c.2), (d.1), (e.1), (d.2) and (e.2), and every 1 centre for (f.1) and (f.2), per 333 km circle per season. Solid lines for positive differences and dashed lines for negative differences.

Simulating global climate in historical times using a coupled atmosphere-ocean general circulation model with all relevant forcings

Martin Stendel (mas@dmi.dk), Irene A. Mogensen and Jens H. Christensen
Danish Meteorological Institute, Lyngbyvej 100, 2100 Copenhagen, Denmark

A meaningful simulation of the climate of past centuries has to take into account all relevant forcings. We have undertaken such a simulation of the climate of the last five centuries with the state of the art coupled atmosphere-ocean general circulation model ECHAM4-OPYC (Stendel et al., 2006). The model has been driven with natural (solar variability, volcanic aerosol) and anthropogenic (greenhouse gases, sulfate aerosol, land-use changes) forcings. In contrast to previous studies, we have taken into account the latitudinal dependence of volcanic aerosol (Robertson et al., 2001) and the changing land cover for a period covering several centuries (Klein Goldewijk, 2001). The experiment has been conducted with the relatively high horizontal resolution of T42. The concentrations of greenhouse gases and CFCs has also been taken from Robertson et al., while solar irradiance variability is based on the updated data set of Lean et al. (1995). Compared to the much-discussed large volcanic forcing of Zorita et al. (2004), the volcanic aerosol load in our simulation is considerably smaller, with the exception of the unknown volcano of 1809 and of Tambora 1815. Changes in land use affect the solar part of the volcanic forcing, and we have made an attempt to calculate the long wave part for historical eruptions as well by estimating the increase of stratospheric temperature due to the aerosol (Andronova et al., 1999). However, there is no feedback to model dynamics.

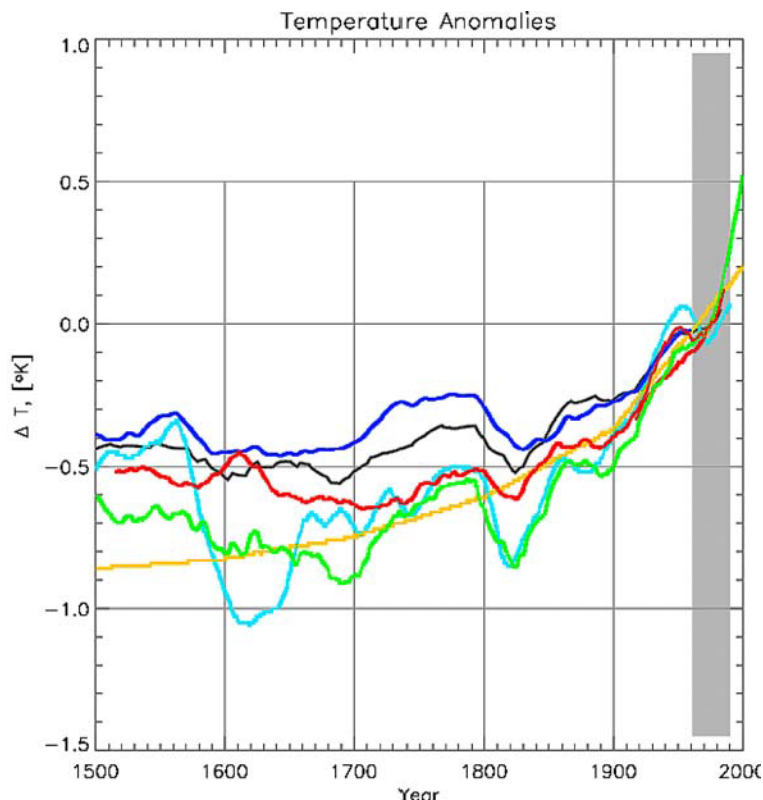


Fig. 1: Thirty-year running averages of near surface temperature anomalies 1500–2000 for the instrumental record (brown curve), the reconstructions of Huang et al. (2000, yellow curve), Esper et al. (2002, light blue) and Mann and Jones (2003, dark blue), the model simulations of Crowley (2000, black) and Zorita et al. (2004, green) and Stendel et al. (2006, red curve).

Fig. 1 shows that we, nevertheless, find a clear signature of large volcanic eruptions in the simulated temperature record. The model is able to simulate individual extreme events such as the “year without a summer” 1816. Strong warming is simulated after 1850, in particular over land, going along with an increase of the positive NAO phase. Consistent circulation anomalies are simulated in multidecadal means with similarity to observed and reconstructed anomalies, for example during the late 17th and early 18th century. The model is able to reproduce some of the observed or reconstructed regional patterns. Cooling during the Late Maunder Minimum is smaller than in other studies, due to the relatively small variations in solar activity and the relatively modest volcanic forcing applied here.

Colder than average conditions, for example during the late 17th and early 18th centuries, go along with a decrease in pressure difference between low and high latitudes and a decrease of the North Atlantic Oscillation. This favours positive sea ice anomalies east of Greenland and around Iceland, leading to widespread negative temperature anomalies over Europe. We also find characteristic blocking patterns over Western Europe, in particular during autumn which contribute to the advection of cold air (Fig. 2).

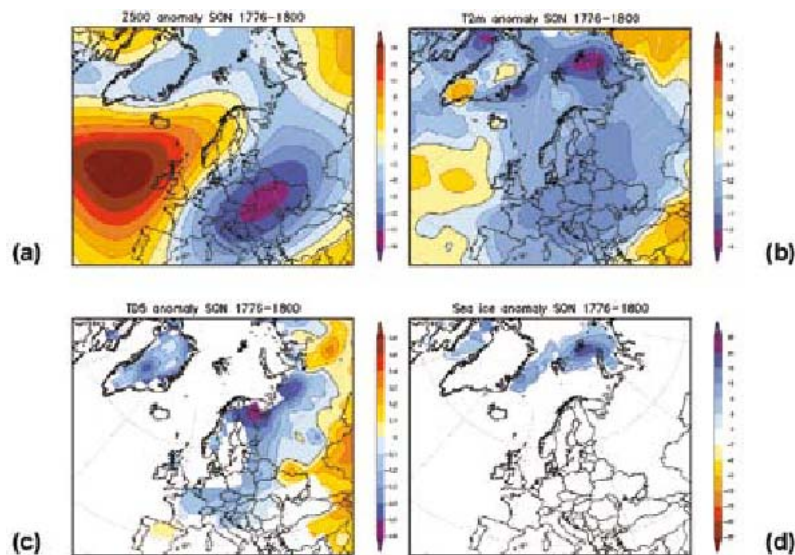


Fig. 2: Twenty-five-year (1776–1800) autumn (SON) anomalies from the 200 year mean 1500–1700 for (a) 500 hPa geopotential (gpm), (b) 2m temperature (K), (c) deep-soil temperature (K) and (d) sea ice cover (%).

References:

- Andronova, N.G. et al., 1999: *J. Geophys. Res.* **104**, 16807-16826
 Crowley, T.J., 2000: *Science* **289**, 270-277.
 Esper, J., Cook, E.R. and Schweingruber, F.H., 2002: *Science* **295**, 2250-2253.
 Huang, S.H., Pollack, N.H. and Shen, P.Y., 2000: *Nature* **403**, 756-758.
 Klein Goldewijk, K., 2001: *Glob. Biogeochem. Cycl.* **15**, 415-433.
 Lean, J., Beer, J. and Bradley, R., 1995: *Geophys. Res. Lett.* **22**, 3195-3198.
 Mann, M.E. and Jones, P.D., 2003: *Geophys. Res. Lett.* **30**, doi: 10.1029/2003GL017814.
 Stendel, M., Mogensen, I.A., Christensen, J.H., 2006: *Clim. Dyn.* **26**, 1-15.
 Zorita, E. et al., 2004: *Met. Z.* **13**, 271-289.

Numerical Experiments of Typhoons in 2004 typhoon season using a non-hydrostatic atmospheric model coupled with a mixed-layer ocean model

Akiyoshi Wada

Meteorological Research Institute, Tsukuba, Ibaraki, 305-0052, Japan
E-mail:awada@mri-jma.go.jp

1. Introduction

Wada (2005a) has developed the non-hydrostatic atmospheric model coupled with a mixed layer ocean model. The coupled model successfully reproduced sea surface cooling (SSC) on the rightward of the moving direction by typhoons. The suppression of typhoon intensity caused by the SSC was successfully simulated in the case of Typhoon Bilis (T0010). The suppression by ocean coupling was more salient using the coupled model with finer horizontal resolution. In the present report, numerical experiments are performed in the cases of six typhoons making landfall on Japan in 2004. A role of ocean coupling on the intensification or maintenance of typhoons is addressed here.

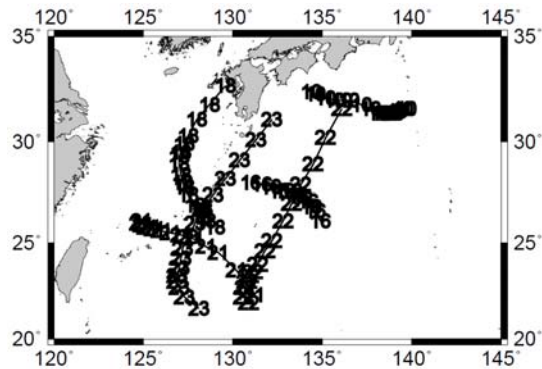


Figure 1 Positions analyzed in Japan Meteorological Agency of six typhoons in 2004 typhoon season.

2. Typhoons in 2004 typhoon season

In 2004 typhoon season, ten typhoons made landfall on Japan, which brought dreadful disasters by destructive wind and torrential rain. Here, six typhoons (T0410, T0416, T0418, T0421, T0422, and T0423) are numerically investigated. Figure 1 shows typhoon tracks during the period of integration (every typhoon is calculated during 48 hours). All the typhoons passed by in the western north Pacific where SSC appeared notably (Wada, 2005b). As for the development stage of T0423, Wada (2005c) suggested that the suppression of minimum central pressure (MCP) was notable in the case of SST lower than 28°C, while the MCP did not appear in the case of SST higher than 28°C even in the coupled experiment in spite that SSC of about 1°C could be reproduced. In contrast, all the stages of six typhoons are in maintaining or decaying stage. According to the result of singular value decomposition analysis in Wada (2005b), six typhoons can be divided into two categories; summer typhoons (T0410, T0416, T0418) and autumn typhoons (T0421, T0422, T0423). In the summer season, solar radiation dominates the SST variation, while the effect of solar radiation on the SST variation is smaller in the autumn season.

3. Numerical experiments

The specification of numerical experiments is almost the same as Wada (2005a) except for the oceanic initial condition, sea spray parameterization and cumulus parameterization. The initialization of oceanic condition is the same as Wada (2006). The sea spray parameterization and cumulus parameterization are not incorporated into the present specification. Horizontal resolution of the model is 6km with 391x391 grids and 40 vertical layers. The integration time is 48 hours. The reanalysis SST by the MRI Ocean Variational Estimation (MOVE) system (Usui et al., submitted) is used in the numerical experiment

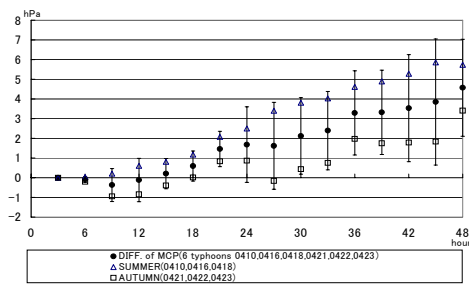


Figure 2 Difference of minimum central pressure between in coupled and non-coupled experiments.

4. Results

4-1 Intensity predictions

Figure 2 shows differences of MCP between in coupled and non-coupled experiments. Except for T0410 case, there is a tendency of underestimation of MCP in comparison with analyzed MCP in Japan Meteorological Agency (JMA). The maximum averaged difference of 6 typhoons is about 4.6hPa at T+48h. The difference of MCP in the summer season is more evident than that in the autumn season. This suggests that ocean coupling effect is a minor role to determine the intensity of

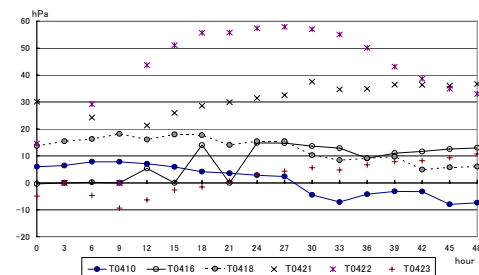


Figure 3 Difference of minimum central pressure between in coupled experiment and best track one.

autumn typhoons.

4.2 Track Predictions

The effect of ocean coupling on the track is shown in Figs.3. The errors from the JMA best track position (Fig. 3(a)) are larger than deviations between the coupled and non-coupled experiments. The improvement of ocean coupling for track prediction is negligibly small (Fig. 3(b)). However, systematic differences of typhoon positions appear in the latter integration in the case of T0410 experiment (not shown).

4.3 Heat flux and precipitation

The ocean coupling effect is evidently found in latent heat flux and accumulated precipitation within a radius of 100km from the typhoon center (not shown). The impact of ocean coupling on latent heat flux and precipitation appears nearest the typhoon center particularly in the early integration. However, this is not always found in the later integration because asymmetrical distribution of latent heat flux and precipitation appears obviously in the typhoons during mature and decaying stages.

4.4 Tropical cyclone heat content

Tropical cyclone heat content (TCHP) is often used to predict the tendency of change of MCP although there was only a few investigation concerning with the relationship between TCHP and intensity of typhoons. Here, we focus on accumulated TCHP, which is defined as summation of TCHP within a radius of 100km from the center every hour. As the mixed layer deepens by entrainment, the SSC around the typhoon center is enhanced (Fig. 5). At that time, TCHP and accumulated TCHP decrease and the difference of MCP in coupled and non-coupled experiments increases (Fig. 5). The tendency of changes of TCHP or accumulated TCHP is notably correlated with that of MCP. Figure 6 indicates the relationship between the tendency of MCP and that of accumulated TCHP, which shows good correlation between them.

However, MCP in T0416 does not fall exceptionally in spite of positive tendency of accumulated TCHP. This suggests that TCHP could not be a dominant factor to determine the intensity of the typhoon. The other physical processes particularly in the atmospheric model, initial and boundary conditions in the atmosphere and oceanic initial condition may be more important for typhoon predictions. The relationship between multi-scale interaction of typhoons and their TCHP conditions will be a future subject of typhoon intensity prediction.

References

- Wada, A., 2005a: Numerical Experiments of Typhoon Bilis Using a Non-Hydrostatic Atmospheric Model Coupled with a Mixed-Layer Ocean Model. WMO, CAS/JSC WGNG Report.
- Wada, A., 2005b: Interrelationship of landfall of typhoons on Japan, sea surface temperature, atmospheric environment, and ocean heat content in 2004. Kaiyo monthly, 42. 30-39. *(In Japanese)*.
- Wada, A., 2005c: Relationship between maintenance of typhoon intensity and sea surface cooling by typhoon using satellite observations and a non-hydrostatic atmospheric model coupled with a mixed-layer model. Kaiyo monthly, 42. 203-211 (In Japanese).
- Wada, A., 2006: Introduction of a mixed-layer ocean model into the MRI interactive multiply-nested movable mesh tropical cyclone model. WMO, CAS/JSC WGNG Report. *(Submitted)*

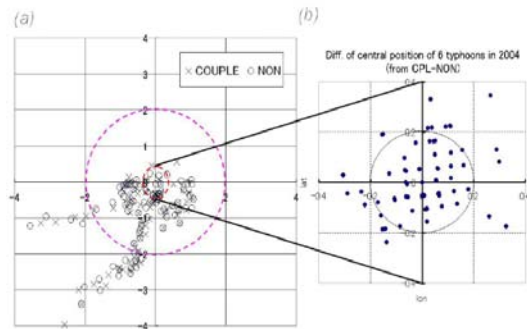


Figure 4 Difference of central position. (a) between in coupled and non-coupled experiment. (b) between in coupled experiment and best track one.

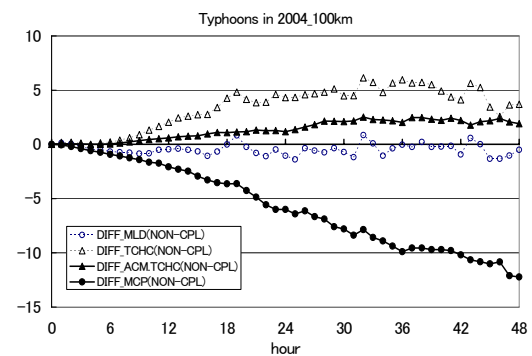


Figure 5 Differences of minimum central pressure, mixed layer depth, TCHP averaged within a radius of 100km from the center, and accumulated TCHP.

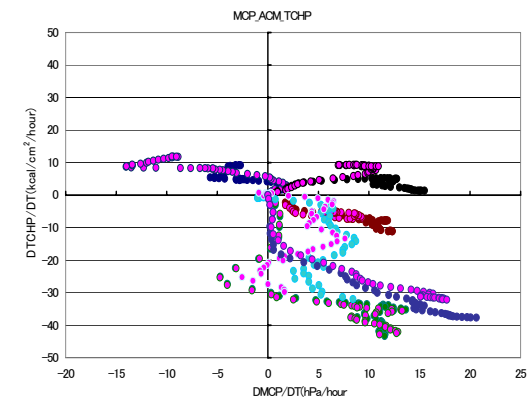


Figure 6 Differences of minimum central pressure, mixed layer depth, TCHP averaged within a radius of 100km from the center, and accumulated TCHP.

Introduction of a mixed-layer ocean model into the MRI interactive multiply-nested movable mesh tropical cyclone model

Akiyoshi Wada* and Wataru Mashiko

Meteorological Research Institute, Tsukuba, Ibaraki, 305-0052, Japan

**E-mail:awada@mri-jma.go.jp*

1. Outline of the MRI tropical cyclone model.

The Meteorological Research Institute (MRI) interactive (or 2-way) multiply-nested movable mesh tropical cyclone model (MRI typhoon model) has been developed for a few years (Mashiko and Muroi,2003) . One of notable features of this model is to possibly simulate detailed structure of tropical cyclones such as the eyewall and rainbands with efficiency for computational resources (e.g. Mashiko, 2005). The model consists of a ‘parent’ main program and some ‘children’ modules written in Fortran language. The algorithm is shown in Fig. 1. The parent model controls some children parts, which the number of children is determined by the number of nest. An interpolation procedure from one nest to another, a procedure of making boundary condition, and setting of domains, all are implemented by the parent main program. Detailed description of the model can be referred to Mashiko and Muroi (2003).

2. Introduction of a mixed-layer ocean model.

A mixed-layer ocean model is introduced into the children parts of the model respectively. Details of the mixed-layer ocean model can be referred in Wada (2005). The mixed-layer ocean model is divided into some module parts as defining oceanic variables, making oceanic initial conditions, defining oceanic topography, forecasting oceanic variables, and outputting results of the time integration every a specified time. Making oceanic initial conditions and spin up procedure are implemented only in the first nest. The initial oceanic fields in the other domains are given by interpolation from the coarse domain of the first nest. One of the noteworthy improvements of the coupled model is to enable computed sea surface temperature (SST) to be interactive between two nests even in the land-sea interface. However, topographic information in both the atmosphere and the ocean in the other domains is determined using model topography with the coarsest horizontal resolution.

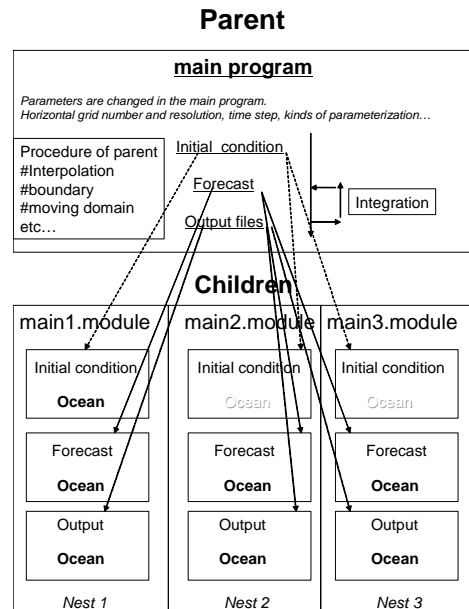


Figure 1. The system of MRI interactive multiply-nested movable mesh tropical cyclone model.

3. Performance of the MRI typhoon model coupled with the mixed-layer ocean model.

3-1 Numerical experiment

A primarily numerical experiment in the case of Typhoon Namtheun (T0410) is performed to check the performance of the MRI typhoon model coupled with the mixed layer ocean model (MRI typhoon-ocean model). The number of nests is set to be two of which horizontal resolutions are 6km (391x391 grids) and 2km (391x391 grids) with 40 vertical layers. To make the initial condition, we run the global spectral model (GSM: T213L40) during 72 hours at first. After that, we further run the hydrostatic typhoon model (TYM) with 20km horizontal resolution and 40 vertical layers during 72 hours using the GSM output as initial and boundary conditions in order to downscale the initial condition. The initial time of GSM and TYM is at 12UTC on July 28. In the experiment of the MRI typhoon model, the initial time is at 00UTC on July 29, T+12hour integration time of TYM where T indicates the initial time of TYM. As for the oceanic initial condition, reanalysis data of sea

temperature and salinity by the MRI Ocean Variational Estimation (MOVE) system is used. The initial mixed layer depth is analyzed from MOVE data. In the present study, the data on July 27, 2-day before the initial time of the initial time, is used as the oceanic initial condition. As for the physics of the MRI typhoon-coupled model, sea spray parameterization is included in the speculation of numerical experiments, but cumulus parameterization is not included in it.

3-2 Results

Figures 2 show horizontal distributions of SST and 1-hour precipitations in the cases of coupled experiments (Fig.2 (a), (b), (d), and (e)) and uncoupled experiments (Fig. 2. (c) and (f)). In northeastward region from the typhoon center, sea surface cooling (SSC) appears notably (Fig.2 (a)). T0410 with concentric and symmetric-like precipitation in the nest with 6km horizontal resolution (Fig.2 (d)) is located southwestward of high pressure in the north Pacific. In the experiment with 2-km horizontal resolution, the SSC appeared in the coupled experiment with 6km horizontal experiment is remarkably evident on the northeastward of the typhoon, which the SSC is located in the rightward of the moving direction (Fig.2 (b)). This SSC does not appear in the non-coupled experiment (Fig.2 (c)). The other notable feature in the experiment with 2km horizontal resolution is that 1-hour precipitation pattern in the coupled experiment (Fig.2 (e)) is different from that in the uncoupled model (Fig.2 (f)). This suggests that ocean coupling could affect not only intensity of the typhoon but also precipitation pattern of it.

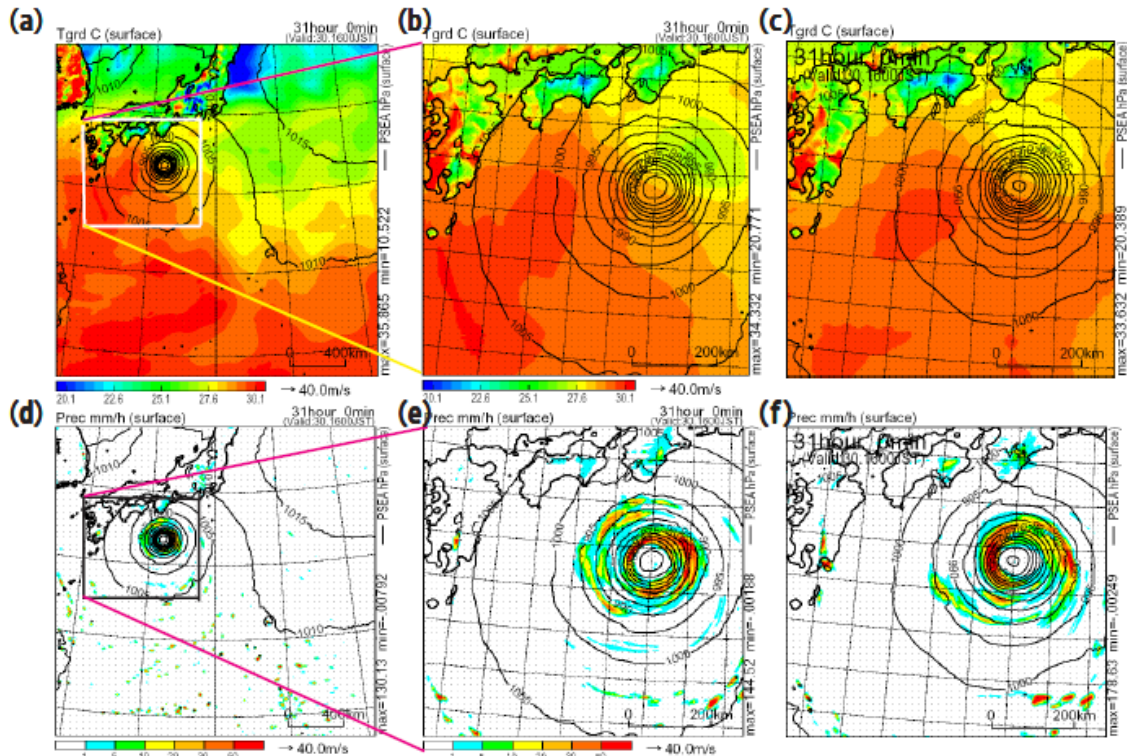


Figure 2 Distributions of SST and precipitation by the MRI typhoon-ocean coupled model. (a) SST with 6km horizontal resolution in the coupled experiment. (b) same as (a) except for 2km horizontal resolution. (c) same as (b) except for one in the non-coupled experiment. (d) same as (a) except for 1-hour precipitation. (e) same as (b) except for 1-hour precipitation. (f) same as (c) except for 1-hour precipitation.

References

Mashiko, W and C. Muroi, 2003: Development of a two-way multiply-nested movable mesh typhoon model using the cloud resolving nonhydrostatic model. WMO, CAS/JSC WNGG Report.
Mashiko, W, 2005: Polygonal Eyewall and Mesovortices Structure in a Numerically Simulated Typhoon Rusa. SOLA, 1, 29-32.
Usui, N., S. Ishizaki, Y. Fujii, H. Tsujino, T. Yasuda and M. Kamachi: Meteorological Research Institute Ocean Variational Estimation (MOVE) System: Some Early Results, *J. Adv. Space Res.* (submitted)
Wada, A, 2005: Numerical Simulations of Sea Surface Cooling by a Mixed Layer Model during the Passage of Typhoon Rex. *J. Oceanogr.* 61. 41-57.

Numerical Experiments of Typhoon Namtheun (T0410) using different atmosphere-ocean coupled models

Akiyoshi Wada

Meteorological Research Institute, Tsukuba, Ibaraki, 305-0052, Japan
E-mail:awada@mri-jma.go.jp

1. Observation in Typhoon Namtheun (T0410)

Typhoon Namtheun (T0410) is one of the typhoons making landfall on Japan in 2004 typhoon seasons. During the mature stage, the distribution of 1-hour precipitation changed from the symmetric pattern (Fig. 1(a) and (b)) to asymmetric one (Fig.1(c) and (d)). At that time, salient sea surface cooling (SSC) appears on the rightward of the track (Fig.2). The area where low temperature appears within the eyewall is located south of the center of the typhoon (Figs.1), which is opposite of SSC. The relationship between asymmetry of 1-hour precipitation and that of SSC is investigated numerically using atmosphere-ocean coupled models with different specifications.

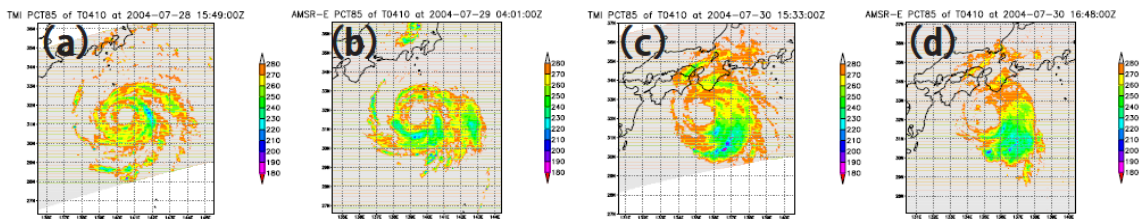


Figure 1 The polarization corrected temperature (PCT) derived from 85GHz channels by TRMM/TMI ((a) and (b)) and AMSR-E ((c) and (d)), (a) at 1549UTC on July 28, (b) at 0401UTC on July 29. (c) at 1533UTC on July 30, (d) at 1648UTC on July 30.

2. Results of hydrostatic typhoon-ocean coupled model

The atmospheric part of hydrostatic typhoon-ocean coupled model (TYM) is a spectral model with 20km horizontal resolution and 40 vertical layers. The mixed-layer ocean model coupled with the TYM is a slab model with 0.2 degrees horizontal resolution and 8 vertical layers. Detailed description of the coupled model is referred in Wada (2003) except for 25 vertical layers in Wada (2003). The initial time of numerical integration is at 12UTC on July 28 in 2004. As for the oceanic initial condition, the analyzed SST by Numerical Prediction Department in Japan Meteorological Agency (JMA) is used. Although the location of SSC by the coupled model (Fig. 3) is different from that by TRMM/TMI SST because of the error of track prediction, the SSC by the coupled model is evident on the rightward of moving direction. Horizontal distribution of sensible plus latent heat flux shows that the maximum heat flux appears ahead of moving direction of T0410, while the minimum appears behind the typhoon (Fig. 4).

The location of maximum heat flux is different from that in the non-coupled experiment (not shown), which the maximum is evident on the rightward of the moving direction. Asymmetric distribution of cloud water content, which the maximum appears southeastward of the typhoon center, is evident at a level of 500hPa (Fig. 5) where air temperature is under 0°C and ice particles coexists in the air. In the non-coupled experiment, the pattern of cloud water content is rather like symmetry (not shown).

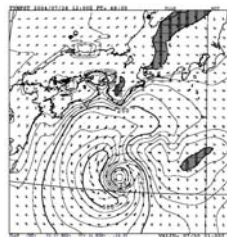


Figure 4 Sensible plus latent heat flux by the coupled model at T+48h.

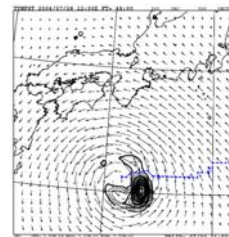


Figure 5 Cloud water content at a level of 500hPa by the coupled model at T+48h and center positions of the typhoon.

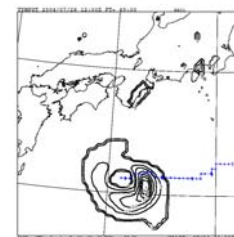


Figure 6 1-hour precipitations by the coupled model at T+49h and center positions of the typhoon.

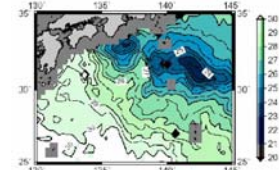


Figure 2 TRMM/TMI 3-day average SST on July 31 in 2004.

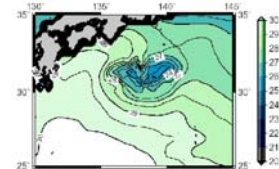


Figure 3 SST by the coupled model at T+48h.

The 1-hour precipitation pattern at T+49h is similar to the pattern of cloud water content at T+48h. In the TYM, precipitation is determined from the cloud water content using the empirical formula of Sundqvist (1978). The Coalescence and Bergeron-Findeisen effects (Sundqvist et al., 1989) may enhance the transformation from cloud water to rain or snow in the eyewall where upward flow is salient. This suggests that the cloud water content affected by SSC determines the asymmetric pattern of precipitation in the TYM-ocean coupled model.

3. Results of non-hydrostatic atmosphere-ocean coupled model

The non-hydrostatic atmosphere-ocean coupled model is referred to Wada (2005). The initial time of numerical integration is at 00UTC on July 29 in 2004, which is 12-hour later than that in the TYM-ocean coupled model. The reanalysis SST by the MRI Ocean Variational Estimation (MOVE) system (Usui et al., submitted) is used in the numerical experiment, which is different from that of TYM-ocean coupled model.

Results of track predictions indicate that northward deflection of the typhoon track is simulated, which is closer to JMA best track positions than that of TYM-ocean coupled model. In addition, the ocean coupling has the track deflect further northward. The difference of minimum central pressure in between coupled and non-coupled experiments is smaller than that of TYM-ocean coupled model (Wada, 2003). However, the intensity is overestimated even in the coupled simulation.

The SSC (Fig. 9) is comparable to TRMM/TMI SSC (Fig. 2), which the SSC appears south of Kii peninsula. The SSC can be successfully simulated in comparison with the result of TYM-ocean coupled model (Fig. 3). The maximum latent heat flux is located in westward of the typhoon center (Fig. 10). This location and asymmetry of the distribution is similar to those in Fig. 4. The decrease of heat flux behind the typhoon also appears in Fig. 10, which is similar to that in Fig. 4. Figures 11 show two kinds of mixing ratio (cloud water (Qc) and rain water (Qr)) at T+36h, total mixing ratio including cold rain elements at T+36h, and 1-hour precipitation at T+37h. The location of broad rainband (Fig. 1(c)) can be successfully simulated in Figs. 11(a)-(c) although the width of rainbands is narrower. The 1-hour precipitation is notable east of the typhoon center (Fig. 11(d)), which is comparable to observation (Fig. 1(c)), too. In the non-coupled experiment, the location of Qc is different from that of Qr. Because Qc is small in comparison with Qr around T0410, the total cloud water is possibly explained from Qr at the height of 5.91km. The Qr, total mixing ratio, and 1-hour precipitation in an hour, all in the non-coupled experiment have the maxima northward from the typhoon center, which make the distribution of precipitation more symmetrical.

In conclusion, the TYM-ocean coupled model, which has coarser horizontal resolution, can simulate suppression of intensification and asymmetry of horizontal distribution of precipitation to an extent. Besides, the non-hydrostatic atmosphere-ocean coupled model, which has finer horizontal resolution, can simulate more detail and realistic distribution of precipitation. The ocean coupling effect may influence the track prediction when the non-hydrostatic atmosphere-ocean coupled model is used. For the purpose of prevention of dreadful disasters by typhoons, the non-hydrostatic atmosphere-ocean coupled model will be required but its computational resource is still expensive. Confined to intensity predictions during a several days, the TYM-ocean coupled model is capable of reflecting the effect of typhoon-ocean interaction on the typhoon prediction.

References

- Sundqvist, H., 1978: A parameterization scheme for non-convective condensation including prediction of cloud water content. *Quart. J. Roy. Meteor. Soc.*, 104, 677-690.
- Sundqvist, H., E. Berge and J. E. Kristjansson, 1989: Condensation and cloud parameterization studies with a mesoscale numerical weather prediction model. *Mon. Wea. Rev.*, 117, 1641-1657.
- Wada, A., 2003: Typhoon-ocean coupled model with upgraded mixed layer model. WMO, CAS/JSC WGNG Report. 09-07.
- Wada, A., 2005: Numerical Experiments of Typhoon Bilis Using a Non-Hydrostatic Atmospheric Model Coupled with a Mixed-Layer Ocean Model. WMO, CAS/JSC WGNG Report. 09-05.

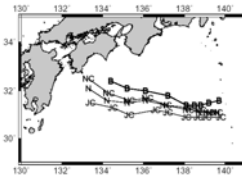


Figure.7 JMA best track positions (B), the predicted positions of hydrostatic coupled model (JC), nonhydrostatic model (N), and nonhydrostatic coupled model (NC).

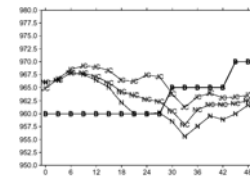


Figure.8 JMA best track minimum central pressure (B), the predicted minimum central pressure of hydrostatic coupled model (JC), nonhydrostatic model (N), and nonhydrostatic coupled model (NC).

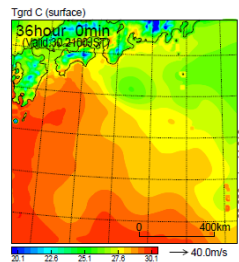


Figure 9 SST by the coupled model at T+36h.

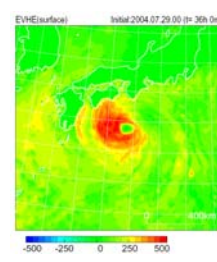


Figure 10 Latent heat flux by the coupled model at T+36h.

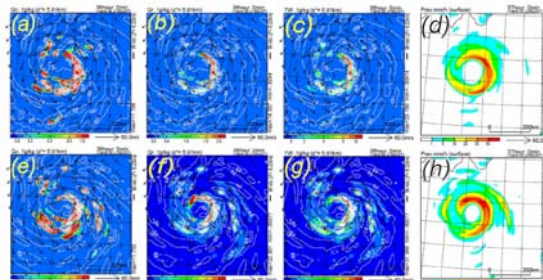


Figure 11 Results of coupled experiment ((a)-(d)) and non-coupled experiment ((e)-(h)) at the height of 5.91km. (a) mixing ratio of cloud water at T+36h, (b) mixing ratio of rain water at T+36h, (c) total mixing ratio at T+36h, (d) 1-hour precipitation at T+37h, (e) same as (a) except for non-coupled experiment, (f) same as (b) except for non-coupled experiment, (g) same as (c) except for non-coupled experiment, (h) same as (d) except for non-coupled experiment.

Typhoon-ocean interaction in Typhoon Megi (T0415) using an atmosphere-mixed-layer ocean coupled model

Akiyoshi Wada

Meteorological Research Institute, Tsukuba, Ibaraki, 305-0052, Japan

E-mail:awada@mri-jma.go.jp

1. Introduction

In general, typhoon-ocean interaction is recognized as suppressing the intensification of typhoons by local sea surface cooling (SSC). However, the interaction does not always occur in numerical experiments. One of the examples is the case of early developing stage of which sea surface temperature (SST) is over 28°C (Wada, 2005a). In this case, moving speed of the typhoon tends to be faster. The fast translation is also seen in typhoons passed by in mid-latitudes where SST is under 28°C. In the present report, we focus on Typhoon Megi (T0415) passed by in the Japan Sea located in mid-latitudes.

2. Numerical experiments

The numerical model using in this study is the non-hydrostatic atmosphere-ocean coupled model (Wada, 2005b). The horizontal resolution is 6km with 252x252 grids with 40 vertical layers. The initial time of numerical integration is at 00UTC on August 19 in 2004. The integration time is 48 hours. The initial and lateral conditions are obtained by interpolation every 6 hours from Meso-Scale Model (MSM) analysis data with 40 vertical layers, which is the same as that of the forecast model. The oceanic initial condition is obtained from reanalysis data by the MRI Ocean Variational Estimation (MOVE) system. Note that T0415 is outside of the computed domain in the initial field.

Results of track prediction and predicted moving speed every 1 hour are shown in Fig. 1. The predicted track is almost the same as the track of Japan Meteorological Agency (JMA) best track during 24-hour in the early integration. The moving speed is nearly 10-15m/s, which is generally faster than that in developing and mature stages. Minimum central pressure (MCP) of the typhoon at T+10h is 980hPa, which is weaker than that of JMA best track MCP of 970hPa. However, the tendency of computed MCP, which shows decaying, agrees well with that of JMA best track during 24-hour in the early integration. This suggests that T0415 is successfully simulated if the integration time is confined within 24 hours.

3. Results

3-1 Sea surface temperature and potential temperature at the lowest level

The difference of SST between the non-coupled and coupled experiments remarkably appears in the Japan Sea, which maximum SSC is over 1°C at T+18h. The maximum SSC is found on the leftward of moving direction, which is opposite of the typical SSC during the passage of typhoons. The difference also appears in potential temperature (PT) at the atmospheric lowest layer of 20m height. At the level, cyclonic but asymmetric circulation where the maximum wind is found around south of the typhoon center is evident. The difference of MCP between non-coupled and coupled experiments does not appear (Fig. 2) in spite of appearance of SSC.

3-2 Surface flux

The ocean coupling effect is evidently found in latent heat flux and accumulated precipitation (Wada, 2006). The

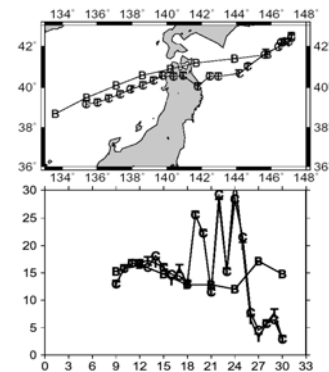


Figure 1 (Upperpanel) Results of track prediction of T0415 every 1 hour in the non-coupled (N), coupled (C), and JMA best track every 3 hours (B). (Lower panel) moving speed of T0415.

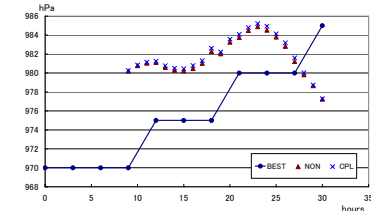


Figure 2 Minimum central pressure of T0415 in the non-coupled, coupled, and JMA best track.

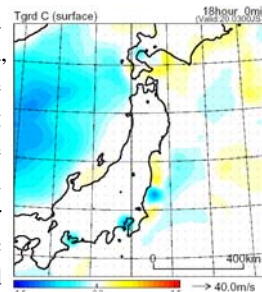


Figure.3 Difference of SST in between coupled and non-coupled experiments.

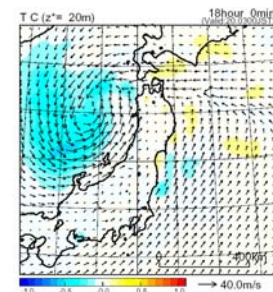


Figure 4 same as Fig. 3 except for potential temperature with surface wind at the lowest level (20m height).

effect appears notably within a radius of 100km from the typhoon center. (Zhu et al., 2004; Wada, 2006). The surface fluxes of mixing ratio of water vapor (Q_v) in both non-coupled and coupled experiments are shown in Figs. 5. Around the center of the typhoon, the surface flux of Q_v is low. The maximum surface flux is found on the leftward of moving direction (Fig. 5(a)). At the region, the decrease of surface flux is salient (Fig. 5(b)) because the region corresponds to the maximum SSC region.

The difference of Q_v and wind velocity in between non-coupled and coupled experiments is shown in Figs. 6. The maximum negative difference of Q_v is found south of the typhoon center where the maximum wind velocity is found (Fig. 4), while the negative difference of wind velocity is salient on the leftward (higher latitudes) of moving direction. The difference of Q_v appeared overall the Japan Sea agrees well with that of SSC by T0415. However, wind velocity at the surface of 20m height does not correspond to the SSC response to PT and Q_v . This suggests that surface wind velocity with cyclonic but asymmetric circulation is influenced by diabatic heating not only around the typhoon center but also in higher latitudes. The process may be related to transformation from a tropical cyclone to an extratropical cyclone.

3-3 Precipitation

The difference of mixing ratio of rain water (Q_r) in between non-coupled and coupled experiments is shown in Fig. 7(a). The pattern of the difference does not correspond to that of PT and Q_v . The deviation is notable in higher mid-latitudes (north of 40N). The difference of accumulated precipitation shown in Fig. 7(b) has a similar pattern to that of Q_r , which is different from the differences typically seen by typhoon-ocean interaction.

4. Related weather event to T0415

During the passage of T0415, air temperature at the surface suddenly rose in Shounai region from 00UTC to 03UTC on August 20. The sudden rising of air temperature during the period is comparable to the temperature by radar-AMeDAS composite analysis. The difference of simulated air temperature in between non-coupled and coupled experiments is negligibly small. This suggests that the sudden rising of air temperature is irrelevant to typhoon-ocean interaction. At Turuoka observing station, simulated air temperature tends to be overestimation. This is partly because of failure of simulating precipitation in Shounai region and positive bias of initial air temperature.

References

Wada, A., 2005a: Relationship between maintenance of typhoon intensity and sea surface cooling by typhoon using satellite observations and a non-hydrostatic atmospheric model coupled with a mixed-layer model. *Kaiyo monthly*, 42, 203-211 (In Japanese).

Wada, A., 2005b: Numerical experiments of Typhoon Bilis using a non-hydrostatic atmospheric model coupled with a mixed-layer ocean model. WMO, CAS/JSC WGNG Report. 09-05.

Wada, A., 2006: Numerical Experiments of Typhoons in 2004 typhoon season using a non-hydrostatic atmospheric model coupled with a mixed-layer ocean model. WMO, CAS/JSC WGNG Report. (Submitted)

Zhu, H., W. Ulrich, and R. K. Smith, 2004: Ocean effects on tropical cyclone intensification and inner-core asymmetries. *J. Atmos. Sci.*, 56, 1245-1258.

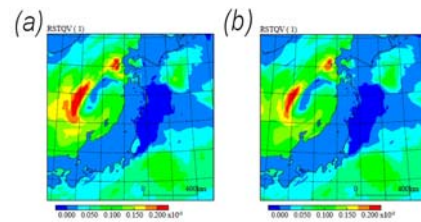


Figure 5 Surface flux of Q_v (a) in non-coupled experiment, (b) in coupled experiment.

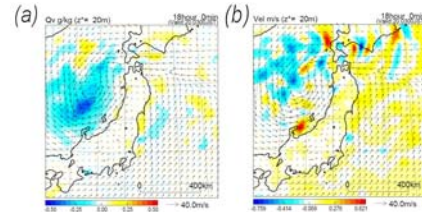


Figure 6 (a) Difference of Q_v at the height of 20m in between coupled and non-coupled experiments, (b) same as (a) except for wind velocity at the height of 20m.

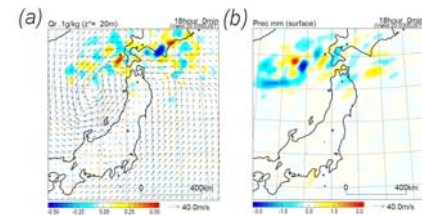


Figure 7 (a) Difference of Q_r at the height of 20m in between coupled and non-coupled experiments, (b) same as (a) except for accumulated precipitation during 18 hours.

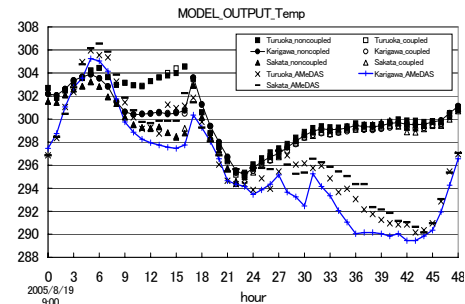


Figure 8 Simulated and observed air temperature at the surface at three observing station (Sakata, Karigawa, and Turuoka) in Shounai region.

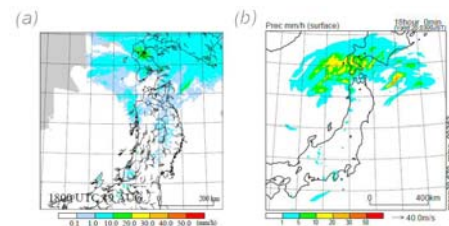


Figure 9 (a) Distribution of 1-hour precipitation and winds at the surface by radar-AMeDAS composite analysis at 18UTC on August 19, (b) distribution of simulated 1-hour precipitation at T+18h.